Numerical Rebuilding of Graphite Ablative Test Case using KCMA

Philippe Reynier

Ingénierie et Systèmes Avancés
16 Avenue Pey Berland, 33600 Pessac, France
Philippe.Reynier@isa-space.eu

ABSTRACT

In the frame of the European Ablation Working Group, test cases based on experimental results obtained for ablative material have been defined in the perspective of a numerical rebuilding with ablation codes. Here, the ablative test case for graphite has been rebuilt using KCMA. This tool is based on a one dimensional approach and uses a surface energy balance at the surface of the material. The results show the capabilities of the tool to recover the evolution trends of the material recession and surface temperature for high-enthalpy tests performed with graphite. However, the tool overestimates the recession at high pressure. The discrepancies between the numerical calculations and the test data might come some experimental errors for the temperature measurements and/or the material properties. Moreover, some improvements could be performed by testing the different correlations for sublimation and oxidation or by accounting for some phenomenon such as nitridation.

INTRODUCTION

In 2005, the European Space Agency has settled, in cooperation with other agencies, research institutes and industry, a European Ablation Working Group (EAWG) [1]. Among the objectives of the EAWG, two are the establishment of a common material database and the improvement of the numerical modelling capabilities. For this purpose, a set of Test Cases, to be numerically rebuilt, has been discussed and defined [2-3]. One of the objectives of the test cases is to define a test matrix covering the different ablation regimes shown in Fig. 1. These regimes depending on temperature and pressure are dominated surface kinetics, diffusion limited and sublimation. Finally, two Test Cases have been selected. The first one is the rebuilding of experiments performed for graphite, while the material chosen for the second test case is the carbon phenolic. Here, the Test Case for graphite is presented with the literature survey used for its definition in the following. Then, the numerical results obtained with KCMA [4] for the test matrix are shown and discussed.

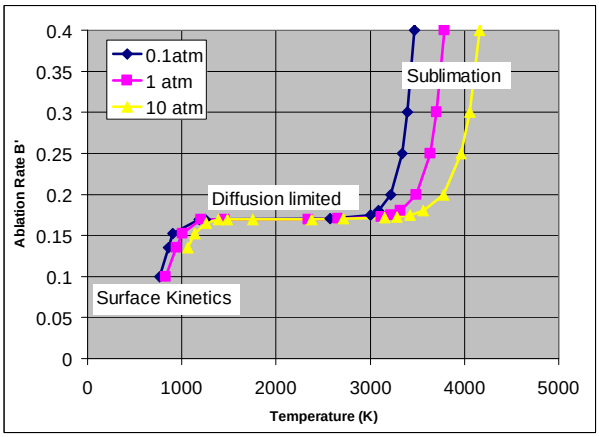

Fig. 1: Dimensionless ablation rate for classical carbon in air with equilibrium assumption as function of temperature [2].

LITERATURE REVIEW

Before the Test Case definition for the graphite, a critical literature review has been performed for the available experimental data obtained with this material [2]. This review has been partially based on a previous literature survey [5] performed on thermal protection system (TPS) materials in 2003, which has been updated and completed when possible.

According to Havstad & Ferencz [6], despite the large number of experimental ablation studies that can be found in the open literature, many done with varying types of graphite, few were reported with sufficient details to be reproduced.

This preliminary review has shown that ATJ graphite was the material with the most complete sets of data; as a consequence it was retained for the Test Case definition.

Table 1: Maah's experimental results [13].

	Experimental results			
Stagnation pressure (atm)	Heating rate (W/cm^2)	Total recession (cm)	Mass-loss rate ($kg.m^{-2}.s^{-1}$)	Surface temperature
0,035	760	0,1612	0,04013	2485
0,6	2073	0,5305	0,20050	3376
2,2	761	0,5016	0,16045	2076
5,6	570	0,4259	0,29906	2085
15	1011	1,0483	0,54860	2579

According to [5] and [6] the more extensive efforts were reported by Maahs [7], Baker et al. [8], Lundell & Dickey [9], Wakefield & Peterson [19], and in the Passive Nosetip Technology Program (PANT) [10-11]. From this list, the studies performed by Baker et al. [8] and in the frame of the PANT were not retained due to the difficulty to access these results, while the works of Auerbach et al. [12] have been added. In order to build the Test Case, the most complete sets of data available in the literature have been reviewed in details. The corresponding studies are those carried out by,

- Lundell & Dickey [9];
- Havstad & Ferencz [6];
- Auerbach et al. [12];
- Maahs [7,13];
- Wakefield & Peterson [14].

The experimental tests of Lundell & Dickey [9] are well documented; nevertheless the surface temperatures reported in this paper do not permit to cover the three ablation regimes shown in Fig. 1. The range of surface temperature covers the diffusion limited and the sublimation regime but not the ablation regime dominated by the surface kinetics that is obtained for surface temperatures below 1500 K.

Havstad & Ferencz [9] have extensively investigated the surface kinetics including CN and CO formation, as well as C_1-C_3, C_5 and C_7 sublimation. Correlations have been proposed for these phenomena that have been validated using PANT experimental data. The range of pressure in the PANT measurements extends up to 250 atm which is much higher than the pressure range retained for the test case (10 atm at the maximum). From the PANT results shown, only the sublimation regime could be covered.

The study of Auerbach et al. [12] was more focused on the graphite porosity. This author gives a distribution of the recession rate versus time for ATJ graphite but with little details on the experimental conditions

Maahs [13] investigated the performance of several materials including two graphites: one pyrolytic and one polycrystalline (ATJ graphite). The experimental results allowed the development of empirical correlations for the mass-loss-rate as function of surface temperature and pressure. The experimental conditions are well described and the sublimation and diffusion limited regimes well covered, whereas the lower range of temperature and pressure is at the limit of the surface kinetics mode.

The same author [7] carried out an investigation on the effects of material properties on the behaviour of 45 different commercial brands of artificial graphite. It was found that the most significant factors affecting graphite performance were the maximum grain size, density, ash content, thermal conductivity and mean pore radius. For optimal performance the grain size should be small, density and thermal conductivity high, ash content low, and the mean pore radius large. This study was performed for only one set of experimental conditions corresponding to the diffusion limited regime.

The results of Wakefield & Peterson [14] cover both diffusion limited and sublimation modes. However, the set of data is not complete for defining a test case. Some data, such as the freestream velocity, the enthalpy and the test duration time are missing. Moreover, most of the tests were performed with a high level of radiative heating rates.

From this critical review of the available data it has been decided to build a test case based on the results available in the NASA report of Maahs [13], which appears to be the most complete. However, a gap exists in the experimental data with little material covering the surface kinetics regime since the low range of surface temperature is not covered as shown in Table 1. Additionally, these tests are old, and today the measurements techniques are more accurate,

particularly if we consider the surface temperature. Additional tests using a more modern material and recent measurement techniques would be very useful to improve this Test Case.

Table 2: Maahs's experimental conditions [13].

Stagnation pressure (atm)	Duration (s)	Nominal total enthalpy (MJ/kg)	Free-stream pressure (atm)	Mach number	Facility
0.035	60	34.9	0.0002	9	HEAT
0.6	45	23	0.23	4.3	HAHT
2.2	60	4.63	0.13	4	HAHT
5.6	30	2.36	0.66	2.5	AHMJ
15	20	2.55	2.43	2.1	CHT

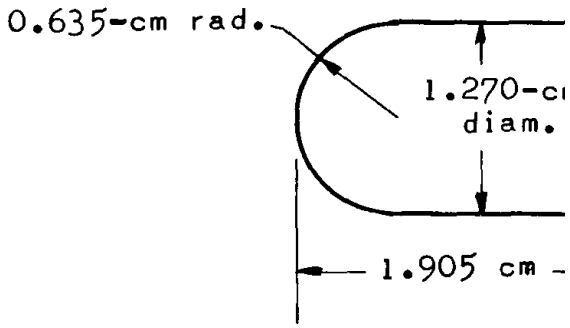

Fig. 2: Schematic diagram of test samples [13].

GRAPHITE TEST CASE

The objective of the Test Case is to rebuild the experiments of Maahs [13] performed with polycrystalline graphite. The experimental test conditions are shown in Table 2. The input parameters have been chosen to insure the best coverage of the different carbon ablation regimes (oxidation, diffusion limited and sublimation) shown in Fig. 1. The main objective of the numerical reconstruction is the prediction of the recession and surface temperature versus test dynamic conditions (cold wall heat flux and stagnation pressure).

The hemispheric geometry of the test sample is shown in Fig. 2. It is a hemispheric cylinder with a diameter of 1.27 cm. The sample is 1.905 cm long with a nose radius of 0.635 cm. The specimen was machined with the across-grain direction parallel to the axis of the specimen. That is, the direction of the lowest thermal conductivity. The sample size is small but this allows reproducing entry conditions in terms of heat-flux and pressure characteristics of an Earth super orbital re-entry. Due to the small size for such samples, the boundary effects are important. As a consequence for the numerical rebuilding, stagnation point calculations will be considered.

The experimental campaigns carried out by Maahs for the polycrystalline graphite were conducted for the range of experimental conditions reported in Table 2. Tests were performed for an air atmosphere, stagnation pressures from 0.035 up to 15 atm and nominal enthalpies from 2.55 up to 34.9 MJ/kg. The corresponding range of surface temperature was between 2000 and 3000 K. All test data was obtained at stagnation point for steady state conditions. The convective cold wall heat flux was related to enthalpy by the equation of Fay and Riddell [15].There was a low radiation environment for the tests without significant radiative heating rate

The values of surface temperature, mass-loss-rate and total recession are reported in Table 1. The distributions of the mass-loss-rate and surface temperature as function of the stagnation pressure are plotted in Fig. 3. In this figure the dash line represent the mass-loss-rate measured at measured at high pressure while the continue line is an extrapolated value (at 15 atm for a shape kept hemispheric).

According to Fig. 1, using these different ranges of pressure and enthalpy, both sublimation and diffusion limited modes are covered. Unfortunately, the surface kinetics regime might not obtained for these conditions due to a too high surface temperature.

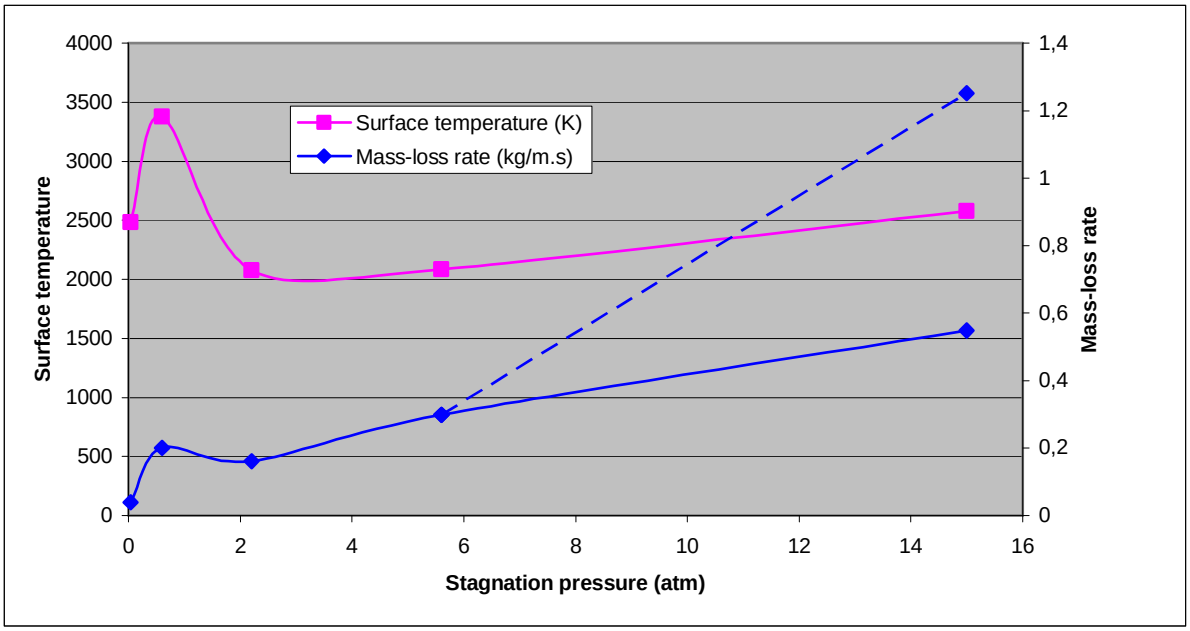

Fig. 3: Surface temperature and mass-loss-rate as function of stagnation pressure in Maahs experiments.

Fig. 4: Conical shape of the sample after the test with a pressure of 15 atm.

The test performed for a stagnation pressure of 15 atm has shown the presence of mechanical erosion. As illustrated in Fig. 4, at the end of the test, the sample geometry was not hemispheric but conical. This conical shape, with an angle of 50°, reflects the presence of a transitional flow: only a small part close to the stagnation point remained hemispheric. Since the Test Case was initially restricted to laminar flow conditions, the test performed for a stagnation pressure of 15 atm is not part of the Test Case. To resume, the test matrix is based on the tests performed at stagnation pressure of: 0.035, 0.6, 2.2 and 5.6 listed in Table 2. The point at 15 atm is kept as optional.

NUMERICAL MODELLING

The calculations have been performed with the ablation tool KCMA. This one-dimensional ablation tool with the governing equations and the numerical scheme are briefly presented hereafter. Additional details on this tool can be found in Ahn et al [4].

Governing Equations

KCMA is an ablation code with the capability to account for pyrolysis and material porosity. The main variables of the problem are the solid density ρ_r, that can vary for pyrolysing materials, the gas density ρ_g, the velocity of the pyrolysis gas u, the solid internal energy e_s, the gas internal energy e_g and the temperature T. The four balance equations for solid density, gas density, gas momentum and total energy conservation are as follows respectively:

$$\frac{\partial \rho_r}{\partial t} = -R \tag{1}$$

$$\frac{\partial}{\partial t}\left(\varepsilon\rho_g\right)+\frac{\partial}{\partial x}\left(\varepsilon\rho_g u\right)=R+D \tag{2}$$

with,

$$D=\frac{K}{\mu}\left(\varepsilon\rho_g\right)\varepsilon\frac{\partial^2 p}{\partial x^2} \tag{3}$$

$$\frac{\partial}{\partial t}\left(\varepsilon\rho_g u\right)+\frac{\partial}{\partial x}\left(\varepsilon\rho_g u^2+\varepsilon\, p\right)=-\varepsilon\, f+I \tag{4}$$

$$\frac{\partial}{\partial t}\left(\rho_c e_c+\rho_r e_r+\varepsilon\rho_g e_g+\frac{1}{2}\varepsilon\rho_g u^2\right)+\frac{\partial}{\partial x}\left[\varepsilon u\left(\rho_g e_g+\frac{1}{2}\rho_g u^2+p\right)\right]=\frac{\partial}{\partial x}\left(\kappa\frac{\partial T}{\partial x}\right) \tag{5}$$

Where p and f are the pressure and friction forces of the pyrolysis gas respectively, R is the pyrolysis rate (equal to zero for the present test case), I the inertial force, and κ the thermal conductivity. D is the rate of change of pyrolysis gas density by diffusion. In Equation (3) D depends on the viscosity μ of the pyrolysis gas, the void fraction ε and K the permeability.

The equations are split in two groups, one for the solid phase and the other for the gas phase. Each group can be represented by the following general equation:

$$\frac{\partial A}{\partial t}+\frac{\partial B}{\partial x}=C \tag{6}$$

The set of equations is then discretised using a finite difference centred scheme accurate to the first order in time and to the second order in space. Each group of equations is solved by the inversion of a block tri-diagonal matrix. A CFL (Courant-Friedrichs-Lewy) number up to 1000 is used for the gas phase. A 10 to 100 time step integration of the gas phase equations enabled the gas phase to catch up with the solid phase integration.

Recession Rate

For the calculation of the recession rate, two phenomena need to be modelled: carbon oxidation and sublimation. The correlation used by Ahn et al [4] for carbon oxidation is retained. The oxidation rate is described as,

$$R_{oxy}=\rho_{ur}\left(a_1+\frac{H-a_2}{a_3}e^{-a_4+a_5 f_s-a_6 f_s^2}\right) \tag{7}$$

with,

$$f_s=\frac{\rho V}{\rho_s} \tag{8}$$

and,

$$\rho_{ur}=\sqrt{2\rho_s\mu_s\frac{V}{R_n}} \tag{9}$$

Where, a_i is a set of constants given in the definition of the Test Case [2]. H is the stagnation enthalpy, ρ and V are the density and the velocity of the flow respectively, R_n is the probe radius, and μ_s and ρ_s are the stagnation values of the density and dynamic viscosity.

The sublimation rate is calculated in the way selected by Park et al [16]:

$$R_s=\frac{k_w\rho_w\gamma_{C_3}M_{C_3}}{1+0.418\left(\frac{T_e}{T_w}\right)^{0.81}\frac{k_w}{V_{rel}}\sqrt{\mathrm{Re}}} \tag{10}$$

Where T_w is the surface temperature, Re the Reynolds number, T_e the temperature at the boundary layer edge, k the Boltzmann constant, and M_{C3} and m_{C3} the molar and molecular mass of C_3 respectively. The quantities γ_{C3} and k_w are defined as,

$$\gamma_{C3}=\frac{1.9\,10^9}{\rho_w T_w}e^{\frac{-59410}{T_w}} \tag{11}$$

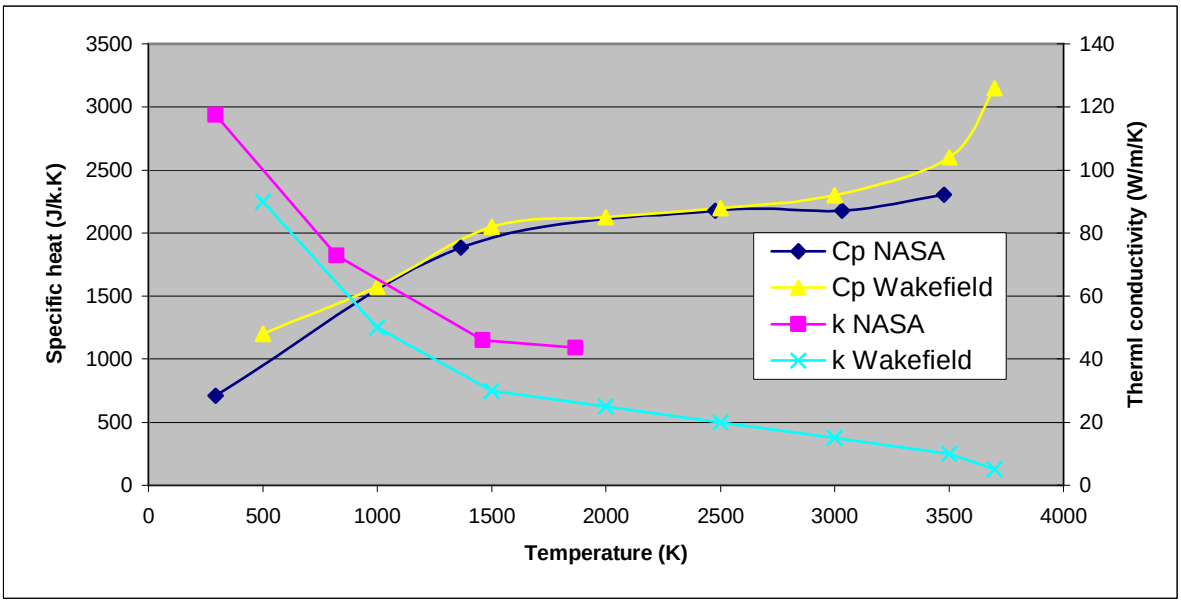

Fig. 5: Curve fits of specific heat and material conductivity obtained with the data of NASA and Wakefield & Peterson.

$$k_w = \frac{1}{4}\alpha_{C_3}\sqrt{\frac{kN_aT_w}{\pi M_{C_3}}} \tag{12}$$

with,

$$\alpha_{c_3} = \frac{30e^{-\frac{21490}{T_w}}}{1+30e^{-\frac{21490}{T_w}}} \tag{13}$$

Where, ρ_w is the wall density and *Na* the number of Avogadro.

Using this modelling some reactions have not been accounted for. Among them, two might play some role: CO_2 production from oxidation or catalysis and surface nitridation.

Thermodynamic Properties

The gas viscosity is calculated using the Wilke's method. The wall temperature and the mixture composition play an important role since the oxidation and the sublimation depends on the quantity of molecular oxygen available in the shock layer. The wall temperature and the mass fraction of the different component of air atmosphere (O, N, N2, O2, NO) are calculated using the hypothesis of a wall at chemical equilibrium. The species mass fraction, temperature and density in the boundary layer are computed using the method of Gordon & Mc Bride and the tables of JANAF [17] and Gurvich [18] for computing the species specific heat, enthalpy and free entropy.

Some thermo-mechanical properties for the material are necessary, such as the specific heat and the thermal conductivity. Available data for ATJ graphite as function of the temperature can be found in [19] and [20]. The distributions of these two quantities as function of temperature are displayed in Fig. 5. The figure shows a good agreement between the data of Wakefield & Peterson [19] and the NASA [20] database for the specific heat below 2700 K, at 3500 K the discrepancy between the two sets is higher than 25%. There is a large difference with a factor two at high temperature for the thermal conductivity (measured in the direction parallel to the flow). Since the set of data for the thermal conductivity provided in [20] is not valid above 2000 K, the choice is done to use, for the Test Case, the values of the thermal conductivity and heat capacity measured by Wakefield & Peterson [19].

NUMERICAL PREDICTIONS

The test matrix shows in Table 1 has been numerically rebuilt (including the case at 15 atm that is not part f the test case) with KCMA using the selected modelling. The computed surface temperature and TPS recession are plotted in Fig. 6 and 7 respectively. A good agreement is found for the prediction of the recession at low pressure and high enthalpy when the thermochemistry effects are significant with more likely some chemical non-equilibrium. At this

regime a strong oxidation is observed and some sublimation is present. The agreement is poor for at high pressure, the flow is without strong chemistry effects with little dissociation.

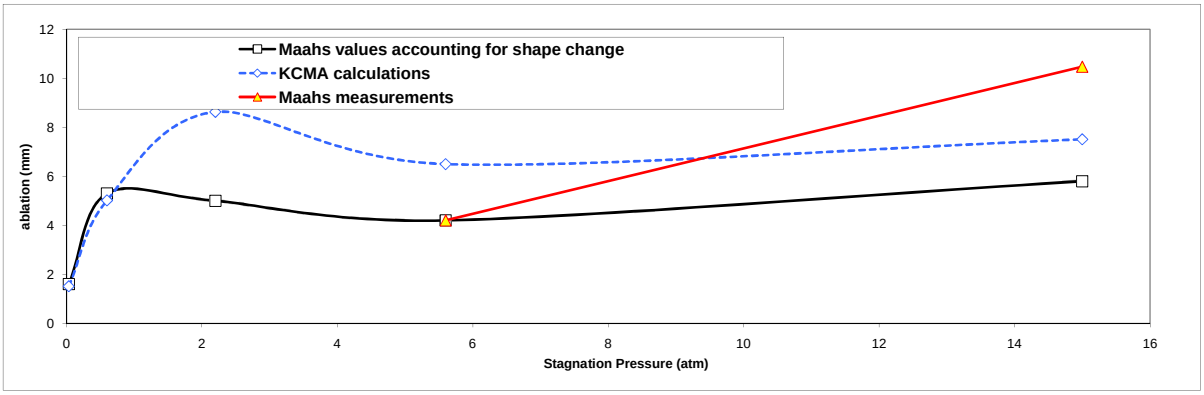

Fig. 6: Experimental data and numerical predictions of the surface temperature.

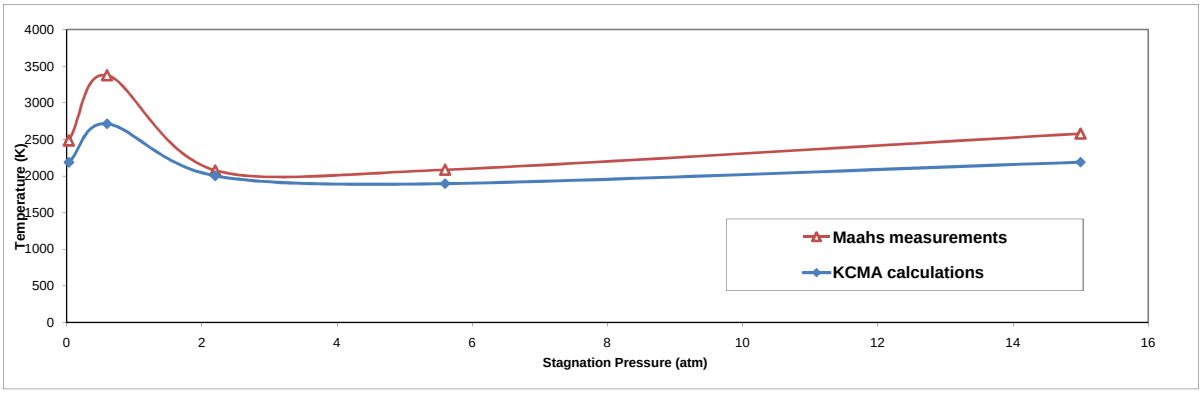

Fig. 7: KCMA calculations and experimental data of the surface recession

These results for the prediction of the recession rate seem to demonstrate that the modelling used for the calculations is more adapted for low pressure and high enthalpy flows. Some additional efforts with other available correlations for the predictions of sublimation and oxidation are necessary to close this point. On the other hand, some phenomena such has nitridation and CO_2 production are neglected, however they could play a significant role.

The comparison between the predicted and measured surface temperatures shows that the numerical tool is able to reproduce the evolution trends as function of the stagnation pressure observed experimentally. A fair agreement is obtained with some discrepancies between the measurements and the numerical predictions. They might come from different origins, at first some experimental errors and some incertitude on the material specific heat. The experimental data are old and there were no direct measurements of the surface temperature since this quantity was estimated from picture records. Maahs [13] evaluated that the uncertainty on the emissivity alone was resulting in an uncertainty on the surface temperature of around 100 K. Concerning the material specific heat, the two available sets of data for this quantity, plotted in Fig. 5 show some differences at high temperature. This point correlates well the Fig. 7 in which the discrepancies between the predictions and the experimental data are larger at high temperature.

However, in the perspective of planetary entries the range of stagnation pressure of interest is below 1 atmosphere and the tool with the models retained for the study is capable to fairly predict the TPS recession.

CONCLUSIONS

The Test Case for graphite defining within the EAWG has been numerically rebuilt. For the recession, the tool has the capability to retrieve the evolution trends observed in the experiments at high enthalpy and low pressure. The trends in the evolution of the surface temperature are reproduced but with a significant discrepancy when comparing with the experimental data.

Some differences between the numerical predictions and the measurements are observed, more particularly at high pressure. These discrepancies can have different sources:

- Chemistry assumptions;
- Experimental errors;
- Uncertainties on the material itself such as the presence of moisture and some material properties;

- Modelling errors.

Some additional work on the test case definition would be useful to evaluate the influence of these different issues. In particular, an assessment of the correlations used for sublimation and oxidation is needed for improving the accuracy of the numerical predictions. The use of well known material with the possibility to reproduce tests would be an asset to improve this Test Case.

Acknowledgements

This work has been supported by the European Space Agency through ESA Contracts 065/2006 and 067/2007. The author of this paper would like to thank Mr. Heiko Ritter and Dr Lionel Marraffa from ESA/ESTEC for their valuable advices and suggestions.

REFERENCES

[1] Reynier, Ph., Ritter, H., Maraffa, L., "Ablation Working Group", ESTEC, Noordwijk, October 2005.
[2] Smith, A., J., Ablation Working Group – Preliminary Identification of Test Cases 2nd Ablation Working Group Meeting, ESTEC, May 16, 2006.
[3] Reynier, Ph., and Chambre, G., Test case definition for numerical rebuilding within the European Ablation Working Group, ESA Contract 067/2007, ISA-TN4-2007, Ingénierie et Systèmes Avancés, Oct. 2007.
[4] Ahn, H.-K., Park, C., and Sawada, K., Response of heatshield material at stagnation point of Pioneer-Venus probes, Journal of Thermophysics and Heat Transfer, VOL. 16(3), pp. 432-439, 2002
[5] White, T., & Parnaby, G., Thermal protection system materials and response correlations literature survey, CR036/03, Fluid Gravity Engineering, July 2003.
[6] Havstad, M. A., & Ferencz, R. M., Comparison of surface chemical kinetic models for ablative reentry of graphite, Journal of Thermophysics and Heat Transfer, Vol. 16(4), pp. 508-515, 2002
[7] Maahs, H. G., A study of the effect of selected material properties on the ablation performance of artificial graphite, NASA TN D-6624, March 1972.
[8] Baker, R. L., Covington, M. A., & Rosenblatt, G. M., The determination of carbon thermochemical properties by laser vaporization, High Temperature Materials chemistry Symposium, electrochemical Society, Pennington, NJ, pp. 143-154, 1983.
[9] Lundell, J. H., & Dickey, R. R., Ablation of ATJ graphite at high temperature, AIAA Journal, Vol. 11(2), pp. 216-222, 1973.
[10] Wool, M. R., Passive Nosetip Technology (PANT) Program, ACUREX Corp., Final Summary Report, AD-A019 186, SAMSO-TR-75-220, Los Angeles, June 1975.
[11] Shimizu, A. B., Ferrell, J. E., & Powars, C. A., Passive Nosetip Technology (PANT) Program, Vol. 12, Nosetip Transition and Shape Change Tests in the AFFDL 50 MW Rent Arc, ACUREX Corp., data Report, AD-A020 710, SAMSO-TR-74-86, Los Angeles, April 1974.
[12] Auerbach, I., Lieberman, M. L., Lawson, K. E., Pierson, H. O., Effects of porosity in graphite materials on ablation in arc-heated jets, Journal of Spacecraft & Rockets, Vol. 14(1), pp. 19-24, January 1977.
[13] Maahs, H. G., Ablation performance of glasslike carbons, pyrolitic graphite, and artificial graphite in the stagnation pressure range 0.035 to 15 atmospheres, NASA TN D-7005, December 1970.
[14] Wakefield, R. M., & Peterson, D. L., Graphite ablation in combined convective and radiative heating, Journal of Spacecraft and Rockets, Vol. 10(2), pp. 149-154, 1973
[15] Fay, J. A., & Ridell, F. R., Theory of stagnation point heat transfer in dissociated air, J. Aeronautical Science, Vol. 25(2), pp. 73-85, Feb. 1958.
[16] Park, C., Jaffe, R. L., & Partridge, H., Chemical-Kinetic parameters of hyperbolic Earth entry, Journal of Thermophysics and Heat Transfer, Vol. 15, No.1, pp. 76-90, January-March 2001.
[17] NIST-JANAF Thermochemical Tables, American institute of physics, August 1998.
[18] Gurvich, L. V., Veyts, L. V., & Alcock, L. V., Thermodynamic Properties of Individual Substances, Hemisphere Pub, March 1989.
[19] Wakefield, R. M., & Peterson, D. L., Graphite ablation in combined convective and radiative heating, Journal of Spacecraft and Rockets, Vol. 10(2), pp. 149-154, 1973.
[20] Williams, S. D., & Curry, D. M., Thermal Protection Materials - Thermophysical Property Data, NASA Reference Publication 1289, 1992.